Journal of Materials Chemistry A

Accepted Manuscript

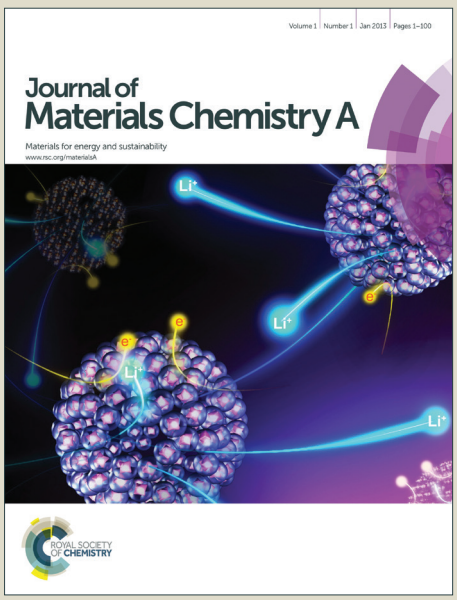

ROYAL SOCIETY OF CHEMISTRY

www.rsc.org/materialsA

Journal of Materials Chemistry A

Journal of Materials Chemistry A

Dynamic Article Links ►

Cite this: DOI: 10.1039/c0xx00000x

ARTICLE

www.rsc.org/xxxxxx

Polyaniline Nanofiber/Electrochemically Reduced Graphene Oxide Layer-by-Layer Elecrodes for Electrochemical Energy Storage

Ju-Won Jeon, Se Ra Kwon and Jodie L. Lutkenhaus*

Received (in XXX, XXX) Xth XXXXXXXXX 20XX, Accepted Xth XXXXXXXXX 20XX

DOI: 10.1039/b000000x

Graphene-containing layer-by-layer (LbL) electrodes are promising for thin film electrochemical energy storage. However, common practice centers on assembly with chemically reduced graphene oxide sheets, which have a tendency to severely aggregate during processing. More direct and facile is the LbL assembly of graphene oxide (GO) sheets and their subsequent electrochemical reduction. Here, we demonstrate porous (void fraction = 0.625) LbL electrodes comprised of electrochemically reduced GO sheets and polyaniline nanofibers (PANI NFs) for use in non-aqueous energy storage systems. Our approach is also promising for deposition onto complex surfaces, as demonstrated here by the successful assembly onto cotton fabric here. Both PANI NFs and ERGO sheets store charge, bear conductivity, and provide a highly porous architecture, which facilitates the mass transport of ions. The nature of PANI NF/GO LbL assembly and growth is first presented, which we find to be affected by assembly pH. The confirmation of the electrochemical reduction step is then discussed, followed by the electrochemical performance of the resulting electrodes in a non-aqueous lithium metal battery. Capacity varies from 85 to 184 mAh/cm^3 (188 to 461 mAh/g) at 0.1 A/g (electrode mass basis), depending on the electrode thickness. The highest specific energy measured was 1395 mWh/g at a specific power of 1590 mW/g, and the highest specific power was 60252 mW/g at a specific energy of 927 mWh/g. These results demonstrate that electroactive polyaniline nanofiber/graphene coatings from aqueous layer-by-layer assembly are attainable for energy storage.

Introduction

Thin film energy storage is growing in importance as demand for micro-power sources in wearable personal electronics, drug delivery, sensors, pacemakers, smart cards, and radio frequency identification (RFID) tags deepens.[1-3] Thin film Li-ion batteries are one such example, in which the electrodes are well below 100 microns in thickness.[4-6] Such examples have been demonstrated in MEMs devices, textiles, acoustic telemetry systems, and conductive paper.[7-10] Thin film energy is also particularly promising for multifunctional structures, where it is desired to integrate energy storage capabilities into a predefined object of interest via advanced coating methods. Another motivation towards thin film energy storage is that materials utilization is enhanced in thin film electrodes because of the reduced diffusion path for ions involved in the redox process.[6] Here, we present a facile route to produce hybrid cathodes comprised of polyaniline nanofibers and electrochemically reduced graphene oxide via layer-by-layer assembly, a conformal coating technique. The result is a water-processable, porous, binder-free, thin film cathode for energy storage capable of coating a variety of surfaces.

Carbon materials such as carbon nanotubes and graphene have been explored as active cathode components, owing to their conductivity and – in some cases - pseudocapacitance.[11-16] Graphene, a two-dimensional sheet of sp^2-hybridized carbon often compared to an un-rolled carbon nanotube, is particularly interesting as an electrode material for thin film batteries because of its high electron mobility, excellent mechanical strength, high thermal conductivity, and high surface area (theoretically up to 2630 m^2 g^{-1}).[17-20] Because of these excellent properties, graphene has been explored in various applications including sensors, solar cells, tissue engineering, drug delivery, and energy storage.[20-25] In energy storage systems, graphene has been widely employed as an electrode material itself or as a conductive additive.[20, 21, 25-27] For example, the conductivity of compressed chemically reduced graphene oxide (CRGO) powder was as high as 200 S/m.[28] Graphene stores charge both via an electric double-layer mechanism and a pseudocapacitive mechanism originating from the rapid redox reaction of oxygen-containing functional groups on the graphene sheet.[16, 29-32] For example, partially reduced graphene oxide electrodes have reported reversible capacities up to 120-200 mAh/g.[16, 33]

Graphene can be prepared using various methods including mechanical exfoliation, chemical vapor deposition, epitaxial growth, and chemical reduction of graphene oxide.[34-38] Chemical reduction of graphene oxide is a particularly promising method because it offers low-cost, large-scale production of CRGO,[38] but processability has been somewhat limited. For example, CRGO is dispersible in some optimized mixed solvents and basic aqueous conditions, but forms irreversible aggregates in neutral and acidic aqueous conditions.[28, 36, 39] This limited processability, originating from CRGO's hydrophobic nature and its relatively low oxygen-containing functional group content, can be circumvented by utilizing graphene oxide (GO) sheets instead. Following GO processing, CRGO product can be obtained using reducing agents such as hydrazine.[39] Recently, the electrochemical reduction of processed GO sheets has been demonstrated, thus eliminating the need for harsh reducing agents.[40, 41]

Polyaniline (PANI), a p-type conjugated polymer, has also been explored as an electrode material for energy storage due to its high theoretical capacity (assuming full doping, neglecting the mass of the anion: 294 mAh/g), good conductivity, low cost, and ease of synthesis.[18, 19, 42, 43] PANI stores charge through a pseudocapacitive doping/dedoping mechanism, in which anions transport in and out of the electrode as PANI is oxidized and reduced, respectively. Accordingly, mass transport of the dopant ion is a potential issue, especially for dense PANI electrodes. In this regard, PANI nanofibers (PANI NFs) are promising because they assemble into porous, high surface area electrodes. PANI NFs can be synthesized rapidly in water, and remain dispersed in a water-processable state for days.[44, 45] PANI NF electrodes exhibited capacities in the range of 75-165 mAh/g as cathodes in non-aqueous cells, demonstrating their ability to store charge.[46, 47]

Layer-by-layer (LbL) assembly is a conformal coating technique recently demonstrated for the formation of thin film battery and supercapacitor electrodes, [29-31, 43, 48-51] and relies upon the alternate adsorption of complementary species from water (or other media).[52] Film properties can be controlled by altering assembly conditions (pH and ionic strength),[53-55] and films can be deposited onto a variety of surfaces (silicon, glass, metal, indium-tin oxide, poly(tetrafluoroethylene)).[48, 56-59] Hammond and Shao-Horn demonstrated high-capacity (200 mAh/g) multiwalled carbon nanotube (MWNT) LbL electrodes, which relied upon charge storage arising from MWNTs' oxygen-containing functional groups.[29] Our group has demonstrated PANI/V_2O_5 LbL battery electrodes with high capacity of up to 264 mAh/g.[43, 60] Elsewhere, PANI/ERGO LbL supercapacitor electrodes were investigated.[51] The PANI/ERGO LbL electrodes possessed a high capacitance of 1563 F/cm^3 (~434 mAh/cm^3 in aqueous media); although these results are promising, the electrodes presented were 70 nm thick. There, the drawback to using conventional PANI was that the PANI/ERGO electrode lacked porosity, leading to electrodes that were functional only when 10s of nanometers thick. Ideally, there should exist some balance between an electrode's thickness, capacity, and materials utilization. Elsewhere, PANI NF/graphene supercapacitor electrodes have been made by dip-coating of graphene sheets followed by electrodeposition of PANI NFs; however, this procedure is cumbersome and not easily automated.[61]

Here, we present assembly of and charge storage in PANI NF/ERGO LbL electrodes for use in non-aqueous thin film batteries. PANI NFs and ERGO sheets both store charge and provide conductivity to the resulting electrode. The PANI NFs produce a porous architecture, thus facilitating mass transport. To date, PANI NF/ERGO LbL electrodes have not been explored as cathodes in non-aqueous batteries. First, this report describes the LbL assembly of PANI NFs and GO sheets, for which pH is used as a tuning parameter for LbL growth. Assembly with CRGO is compared to GO sheets, and it is shown that GO is far more versatile in LbL processing. The resulting PANI NF/GO LbL films were successfully reduced electrochemically. No additional reducing agents or thermal treatments were required. Next, charge storage in PANI NF/ERGO LbL electrodes as battery cathodes in non-aqueous media is presented. Special attention is paid towards charge storage as a function of electrode thickness, in which the highest capacity was 184 mAh/cm^3 (461 mAh/g) for a 460 nm film at 0.1 A/g. It is further shown that polyaniline's stability is enhanced through interactions with ERGO sheets. The electrodes can be conformally coated onto a variety of surfaces, perhaps presenting a suitable approach toward multifunctional energy storage.

Results and discussion

The LbL assembly of PANI NFs and GO sheets was investigated for various assembly pH values, as it has been shown that pH can strongly affect LbL growth.[53, 62] Two different pH values (3.5 and 10) were chosen for the GO dispersion, whereas the pH of the PANI NF dispersion was fixed at 2.5. For LbL assembly, PANI NFs are known to be only stable under acidic aqueous conditions.[45, 48] The zeta-potential of GO sheets is dependent on pH because of abundant oxygen-containing functional groups such as carboxylic acid and phenolic hydroxyls,[39] Figure S1.

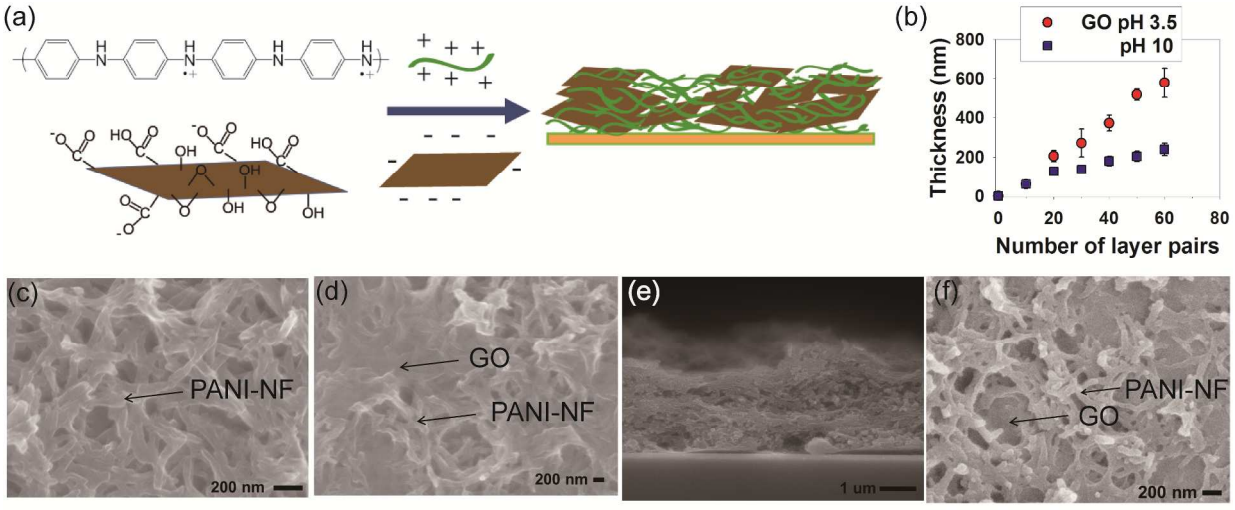

Figure 1. (a) LbL assembly of PANI NFs and GO sheets. (b) PANI NF/GO LbL thickness vs. number of layer pairs measured using profilometry for varing GO pH values. The pH of PANI NFs was fixed at 2.5. (c) Top-view of PANI NFs (d) Top-view and (e) cross-sectional SEM images of (PANI $NF_{2.5}$/$GO_{3.5}$) LbL electrodes. (f) Top-view of (PANI $NF_{2.5}$/$ERGO_{3.5}$) LbL electrodes after electrochemical reduction.

Cite this: DOI: 10.1039/c0xx00000x

www.rsc.org/xxxxxx

ARTICLE

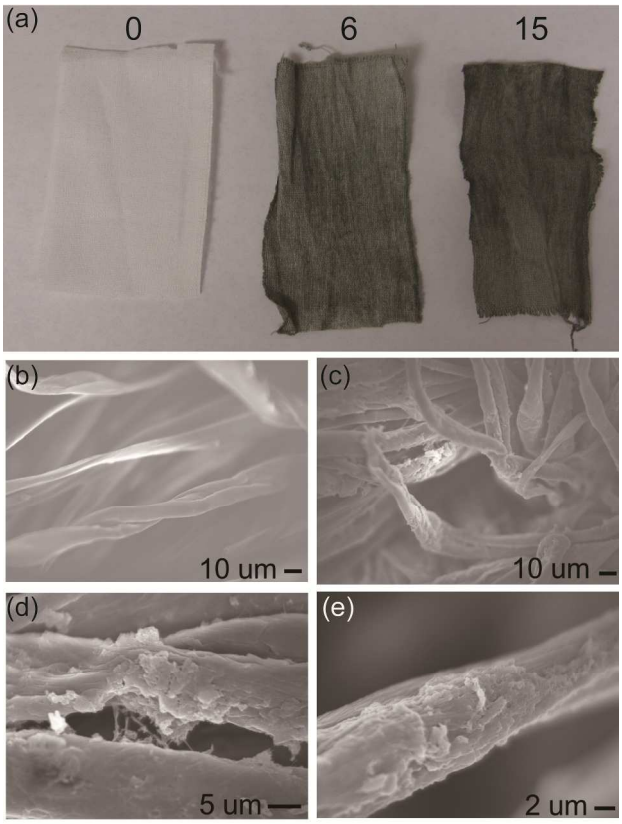

Figure 2. (a) Digital image of PANI NF/GO LbL films on cotton fabric, from left to right (0, 6 and 15 layer pairs). SEM images of (b) bare cotton fabric and (c-e) 15 layer pairs of PANI NF/GO on cotton fabric.

The zeta-potential of GO at pH values 3.5 and 10 was -31 and -43 mV, respectively, and that of PANI NFs was +35 mV; these values show that the nanomaterials are sufficiently charged for LbL assembly.

PANI NF/GO electrodes were built up via LbL assembly, Figure 1a. The resulting films are denoted by (PANI NF_x/GO_y) LbL assemblies, in which the subscripts x and y denote the assembly pH of PANI NF and GO dispersions, respectively. For both assembly conditions, the electrodes were green in color and became successively darker with further cycles of deposition, Figure S2. The green color originated from the conductive emeraldine state of PANI.[48] Successful assembly was further confirmed by the linear increase in thickness per layer pair deposited, Figure 1b. Electrodes assembled at GO pH 3.5 exhibited a larger layer pair thickness (9.6 nm/layer pair) as compared to those assembled at GO pH 10 (4.0 nm/layer pair).

The difference in layer pair thickness probably stems from the variation in GO's surface charge with pH, as supported by zeta-potential measurements. GO sheets at pH 3.5 are less negatively charged as compared to those at pH 10 because carboxylate and phenolic acid groups are more likely to be ionized at higher pH values.[39] Therefore, in the case of less ionized GO sheets (pH 3.5), a larger amount of GO is required to reverse the surface's charge, leading to a larger thickness per layer pair. Similar phenomena have been observed in other LbL systems.[53, 62] For both PANI NF/GO LbL films, the average layer pair thickness was smaller than the PANI NF diameter (ca. 50 nm), which indicates that PANI NF/GO LbL films do not consist of distinctive PANI NF and GO layers. We speculate that this low layer pair thickness originates from patchy adsorption during assembly. The lack of discrete layers, however, may allow for intimate contact between PANI NFs and GO sheets.

We also attempted LbL assembly of PANI NFs and chemically reduced graphene oxide (CRGO) sheets. In this case, the pH of CRGO was maintained at pH 10 or higher because CRGO forms irreversible aggregates in neutral and acidic conditions.[39] However, during the assembly, film delamination and severe aggregation of CRGO occurred, suggesting that stability during LbL deposition is poor, even at pH 10. This finding highlights the apparent challenge of conducting LbL assembly with CRGO sheets. By using GO sheets instead, one can circumvent this challenge.

The composition of PANI NF/GO LbL films was measured using QCM. PANI NFs were the dominant species within (PANI $NF_{2.5}/GO_{3.5}$) LbL films (81 wt% PANI NF and 19 wt% of GO), Figure S3. For (PANI $NF_{2.5}/GO_{10}$) LbL films, it was difficult to obtain reproducible data due to excessive noise in the data. We selected the (PANI $NF_{2.5}/GO_{3.5}$) LbL system for further investigation because its layer pair thickness was sufficiently large so as to build up electrodes in a timely fashion.

SEM images confirm the successful LbL assembly of (PANI $NF_{2.5}/GO_{3.5}$) LbL films, Figure 1c-f and S4. The surface of drop-cast PANI NFs shows a fibrous structure, Figure 1c. In contrast, the surface of the PANI NF/GO LbL assembly bears opaque regions, which are attributed to GO sheets, in addition to PANI NF features. Cross-sectional images of the LbL electrode also exhibit both PANI NFs and GO sheets. No distinguishable stratified layers are observed, consistent with our previous observation of patchy growth, which leads to intimate mixing of the two nanomaterials. The porous nature, arising from the presence of PANI NFs is clearly visible.

The density of a thick (PANI $NF_{2.5}/GO_{3.5}$) LbL system was estimated from QCM and profilometry as 0.56 g cm^{-3}. The void fraction of (PANI $NF_{2.5}/GO_{3.5}$) LbL films was estimated using the following equation:

$$\text{Void Fraction} = 1 - d_{film}/[(\rho_{PANI})(f_{PANI})+(\rho_{GO})(f_{GO})] \quad (1)$$

where d_{film} is the density of the LbL film, ρ_{PANI} is the density of PANI (1.33 g/cm^3), and ρ_{GO} is the density of GO (1.22 g/cm^3), respectively.[63-65] The fraction of PANI (f_{PANI} =0.81) and GO (f_{GO} 0.19), respectively, was obtained from QCM. Therefore, the estimated void fraction was 0.625. This structure is advantageous

Cite this: DOI: 10.1039/c0xx00000x

www.rsc.org/xxxxxx

ARTICLE

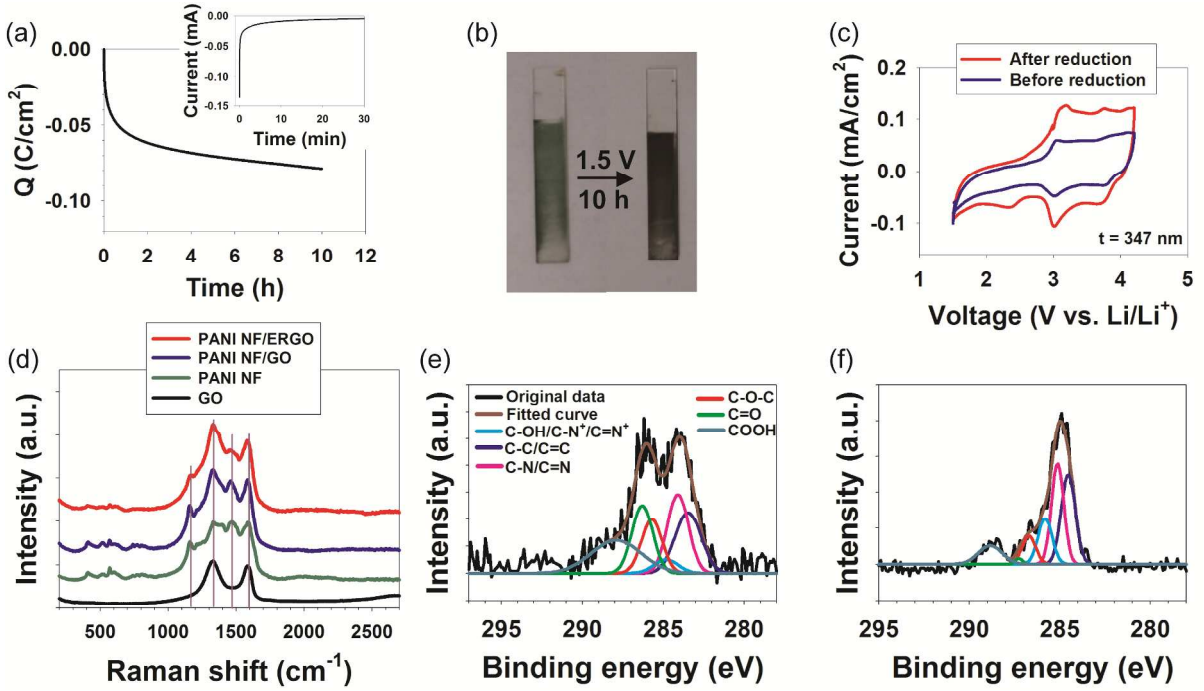

Figure 3. (a) Cumulative charge transferred and current (inset) during electrochemical reduction of a 271 nm thick (PANI $NF_{2.5}/GO_{3.5}$) LbL film at 1.5 V (vs. Li/Li^+), (b) digital images of a 371 nm thick (PANI $NF_{2.5}/GO_{3.5}$) LbL film before and after reduction (the substrate is indium tin oxide (ITO) coated-glass), (c) cyclic voltammograms of a 347 nm thick LbL electrode before and after reduction at 20 mV/s, and (d) Raman spectra of PANI NFs, GO sheets, (PANI $NF_{2.5}/GO_{3.5}$) and (PANI $NF_{2.5}/ERGO_{3.5}$) LbL electrodes. The C1s XPS spectra of (e) (PANI $NF_{2.5}/GO_{3.5}$) and (f) (PANI $NF_{2.5}/ERGO_{3.5}$) LbL electrodes. The legend in panel (e) also applies to panel (f).

Table 1. The composition of C 1s peaks for (PANI $NF_{2.5}/GO_{3.5}$) and (PANI $NF_{2.5}/ERGO_{3.5}$) LbL electrodes.

	C-C/ C=C 284.5 eV	C-N/ C=N 285.1 eV	C-OH/ C-N⁺/ C=N⁺ 285.8 eV	C-O-C 286.7 eV	C=O 287.3 eV	COOH 288.6 eV
PANI NF/ GO	20.4 %	21.6 %	4.3 %	14.3 %	18.2 %	21.2 %
PANI NF/ ERGO	31.6 %	30.9 %	15.9 %	9.5 %	1.1 %	11 %

for charge storage in that it leads to larger surface area and enhanced ion transport relative to a dense non-porous electrode.

The good processability of PANI NFs and GO sheets is further demonstrated by LbL assembly onto cotton fabric, Figure 2. As the number of layer pairs increased, the cotton fabric grew darker in color, indicative of LbL deposition (Figure 2a). In SEM images (Figure 2c-e), the LbL coating on individual cotton fibers was observable, which is in contrast to the bare fabric (Figure 2b), which displayed relatively smooth fiber surfaces.

After assembly, the LbL electrodes were electrochemically reduced at 1.5 V *vs.* Li/Li^+ in an organic electrolyte (0.5 M $LiClO_4$ in propylene carbonate) for 10 h. The purpose of this treatment was to electrochemically convert GO sheets to ERGO in the as-assembled electrode. As compared to conventional chemical reduction, no harsh reducing agents or additional purification steps were required. Figure 3a presents the cumulative charge transferred during the 10 h reduction period. Significant charge transfer was observed within the first hour, after which the amount of charge passed decreased. Similarly, the reduction current was highest at early times and approached zero as reduction continued, Figure 3a inset. Upon electrochemical reduction, the LbL film's color changed from dark green to black, Figure 3b. After electrochemical reduction, the porous structure persisted, Figure 1f.

The electronic conductivity before and after thermal reduction was measured to approximate the change in conductivity brought about by electrochemical reduction. (Four-point probe conductivity measurements of PANI NF/ERGO films were prohibitive because they necessitated deposition onto a conductive substrate). Accordingly, (PANI $NF_{2.5}/GO_{3.5}$) LbL films were thermally reduced at 175 °C for 90 min in air;[66] this process gives XPS spectra similar to our (PANI $NF_{2.5}/ERGO_{3.5}$) samples. The as-prepared (PANI $NF_{2.5}/GO_{3.5}$) LbL films had a conductivity of 5.6 S/m, which is much lower than that of PANI NFs (~ 50 S/m) due to the presence of GO sheets.[67] Upon thermal reduction, the electronic conductivity increased to 125 S/m. After doping with HCl, the conductivity further increased to 184 S/m. We propose that (PANI $NF_{2.5}/ERGO_{3.5}$) LbL electrodes

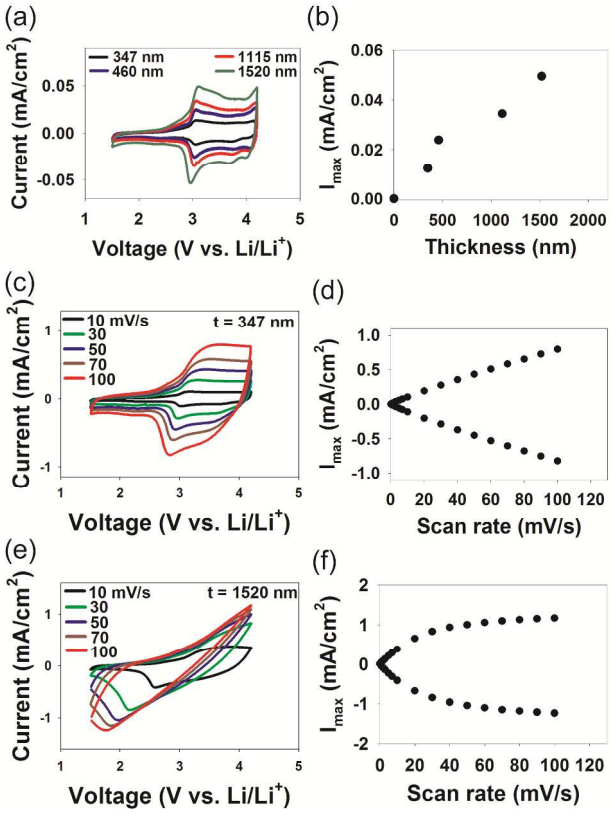

Figure 4. (a) Cyclic voltammograms of (PANI $NF_{2.5}/ERGO_{3.5}$) LbL electrodes of varying thicknesses at 1 mV/s. (b) Maximum current taken from voltammograms shown in panel (a) *vs.* electrode thickness. Cyclic voltammograms of (c) 347 nm and (e) 1520 nm thick (PANI $NF_{2.5}/ERGO_{3.5}$) LbL electrodes at various scan rates. Maximum current *vs.* scan rate for (d) 347 nm and (f) 1520 nm thick electrodes taken from the corresponding cyclic voltammograms.

have conductivity similar to the thermally reduced analogs because of their similar XPS spectra.[66]

Cyclic voltammetry of the electrodes before and after electrochemical reduction provides further evidence for enhanced conductivity, in which the reduced electrode showed a larger current response, Figure 3c. This is consistent with prior reports for which GO electrodes had lower electrochemical activity because of poor electrical conductivity.[16, 33] The change in color, coupled with the increased electrochemical activity, suggests that electrochemical reduction successfully converted GO to ERGO.

Raman spectroscopy was performed to further investigate the electrochemical reduction of (PANI $NF_{2.5}/GO_{3.5}$) LbL films, Figure 3d. For GO, the peaks centered at 1330 and 1580 cm^{-1} were observed, which were ascribed to D and G bands, respectively. The D band arises from defective carbon structures, and the G band is an indication of ideal graphitic sp^2 carbon.[68, 69] The Raman spectra of PANI NFs contains peaks at 1158, 1330-1440, 1480 and 1580 cm^{-1}, attributed to C-H bending, C-N^{*+}, C=N, and C-C stretching, respectively.[30, 70] As expected, (PANI $NF_{2.5}/GO_{3.5}$) LbL films had both peaks from PANI NFs and GO sheets. After electrochemical reduction, all peak positions remained the same; however, the ratio of the D to G band intensities increased from 1.14 to 1.24. This trend has been observed with other chemical reduction methods, in which the increased D/G ratio was attributed to a decrease in the size of sp^2 domains.[28, 71 71-73] Here, it can be inferred that electrochemical reduction results in new graphitic sp^2 domains having smaller sizes relative to the starting materials.

XPS was carried out on PANI NFs, GO sheets, (PANI $NF_{2.5}/GO_{3.5}$) and (PANI $NF_{2.5}/ERGO_{3.5}$) electrodes, Figure 3e-f and Figure S5. The C 1s region for GO sheets had two broad peaks at 284.5 and 286.8 eV, attributed to sp^2 graphitic domains and oxygen-containing functional groups, respectively. In (PANI $NF_{2.5}/GO_{3.5}$) LbL films, similar C 1s peaks were observed, but at reduced intensity for the 286.8 eV peak owing to dilution by the PANI NF component. For the (PANI $NF_{2.5}/GO_{3.5}$) LbL electrode, the C:O atomic ratio increased from 1.97 to 3.76 upon electrochemical reduction of GO to ERGO sheets. The decrease in apparent oxygen content suggests that electrochemical reduction reduces the quantity of oxygen-containing functional groups on the GO sheets.

To further investigate the effect of electrochemical reduction, the C 1s region was deconvoluted into six different Gaussian peaks centered at 284.5, 285.1, 285.8, 286.7, 287.3, and 288.6 eV, attributed to C-C/C=C, C-N/C=N, C-OH/C=N/C-N^+, C-O-C, C=O, and COOH groups, respectively[74-78] (Figure 3e-f and Table 1). The amount of C-C/C=C (arising from sp^2 graphitic domains) increased while the amount of oxygen-containing functional groups generally decreased following electrochemical reduction, indicating the restoration of a sp^2 carbon structure. In particular, ketone groups significantly decreased from 18.2 % to 1.1 % and COOH groups decreased from 21.2 to 11 % after electrochemical reduction. The percentage of C-OH/C-N^+/C=N^+ groups increased upon reduction, the origin of which could be related to increased relative polyaniline content in LbL films. It is known that reduction of GO sheets liberates oxygen-containing functional groups in the form of CO, CO_2, H_2O and O_2.[79, 80] This mass loss from graphene oxide could increase the relative PANI content in LbL films. Overall, these XPS results further confirm the electrochemical reduction of PANI NF/GO LbL films, which is in accordance with Raman spectra.

Thin film electrodes for energy storage are promising because they offer high materials utilization without the need for binders or other additives.[6] However, it can become difficult to transport electrons and ions as the electrode's thickness increases. Therefore, we investigated the performance LbL films of varying thickness, controlled by the number of LbL cycles performed. Further, it has been discussed that performance metrics of thin film electrodes become skewed, trending toward higher values, if reported on a per electrode mass basis; therefore, it is proposed that reporting performance metrics by volume or by area is more appropriate.[3, 81] Here, we present our results in terms of both electrode volume and mass so as to allow proper comparisons with prior literature, some of which reports on a per electrode mass basis.

The electrochemical performance of (PANI $NF_{2.5}/ERGO_{3.5}$) LbL electrodes was assessed in a three-electrode configuration. Before measurements, the electrode was conditioned (one hundred cycles of cyclic voltammetry from 1.5 to 4.2 V at 20 mV/s); this process serves to accelerate the penetration of electrolyte into the electrode, Figure S6. Overlapping cyclic voltammagrams during forward and backwards sweeps was suggestive of the electrode's reversibility, Figure S7. In cathodic scans, two prominent peaks were observed around 3 V and 3.8 V, which are attributed to leucoemeraldine/emeraldine and emeraldine/pernigraniline redox reactions.[48] It should be noted that ERGO provides electrical double layer capacitance as well as additional pseudocapacitance over a wide potential range originating from oxygen-containing functional groups even though no distinctive peak was observed.[29-31, 82]

Cite this: DOI: 10.1039/c0xx00000x

www.rsc.org/xxxxxx

ARTICLE

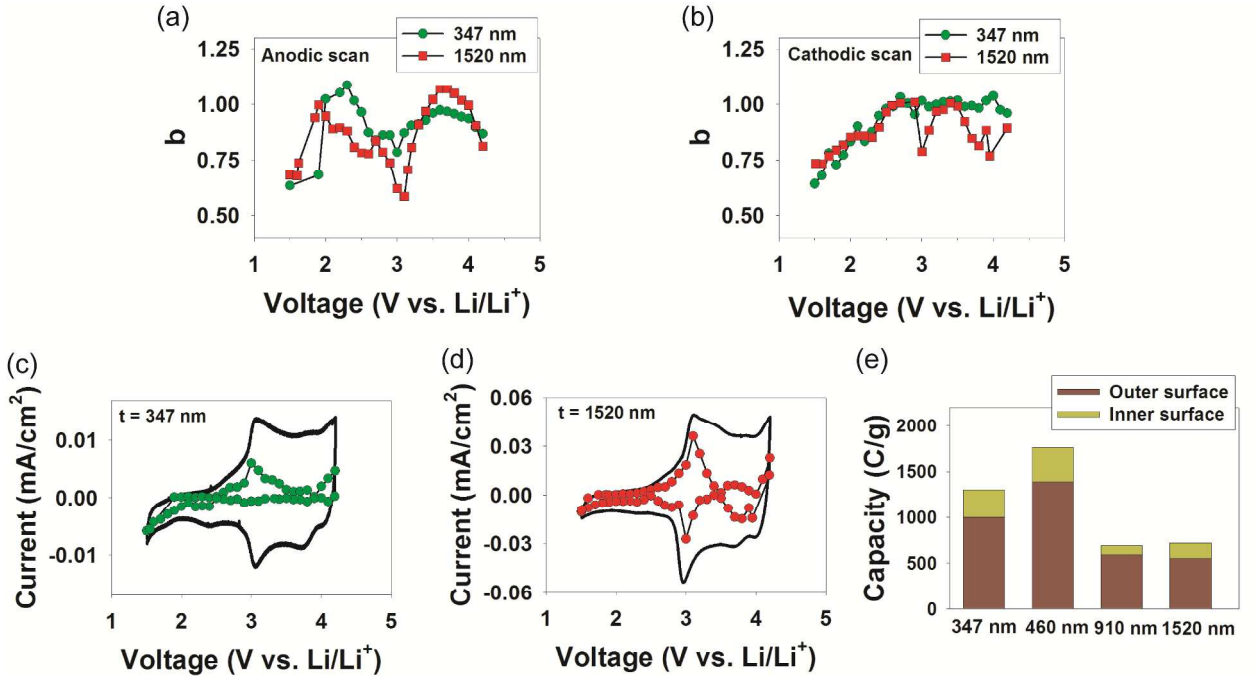

Figure 5. Calculated b values for (a) anodic and (b) cathodic scans of 347 nm and 1520 nm thick (PANI $NF_{2.5}/ERGO_{3.5}$) LbL electrodes *vs.* voltage (b-values were obtained from the equation $i = av^b$ from 1 to 5 mV/s). The diffusion-controlled contribution separated from cyclic voltammograms of (c) 347 nm and (d) 1520 nm thick (PANI $NF_{2.5}/ERGO_{3.5}$) LbL electrodes at 1 mV/s. The dotted line indicates the diffusion-controlled redox processes, and the solid line indicates the total current. (e) Inner and outer surface charge storage depending on the electrode thickness.

In comparison to several other polyaniline-based LbL electrodes,[43, 48] the (PANI $NF_{2.5}/ERGO_{3.5}$) LbL electrodes exhibit greater electrochemical stability. PANI usually loses its electrochemical activity due to irreversible oxidation beyond 3.5 V (*vs.* Li/Li^+) in non-aqueous energy storage systems, as observed in PANI/polyacid, PANI/V_2O_5, and PANI NF/V_2O_5 LbL electrodes.[43, 48, 60] Here, (PANI $NF_{2.5}/ERGO_{3.5}$) LbL electrodes possessed reversible charge storage over a much wider voltage window (1.5 to 4.2 V *vs.* Li/Li^+). We suppose that the interaction between PANI NFs and oxygen-containing functional groups on ERGO sheets suppresses the irreversible degradation of PANI. Previously, we observed that strong interactions between PANI and a strong polyacid via template polymerization also induced electrochemical stability up to 4.5 V *vs.* Li/Li^+.[48, 83] Elsewhere, PANI NF/MWNT LbL electrodes also could maintain reversible charge storage up to 4.5 V (*vs.* Li/Li^+) after heat treatment.[30] Here, we observed good reversibility for (PANI $NF_{2.5}/ERGO_{3.5}$) LbL electrodes without the need for a heat treatment.

(PANI $NF_{2.5}/ERGO_{3.5}$) LbL electrodes of varying thickness were subjected to cyclic voltammetry at 1 mV/s and 30 mV/s in three-electrode cells to assess relationships between charge storage and film thickness, (Figure 4a and Figure S8, respectively). At a scan rate of 1 mV/s, no significant peak shift was observed in anodic and cathodic peaks as electrode thickness increased, and current response nearly linearly increased with thickness at 1 mV/s, Figure 4b. On the contrary, at a scan rate of 30 mV/s, the two cathodic peaks substantially shifted and overlapped as electrode thickness increased, Figure S8. This result suggests that all of the electrode material is accessible and that ion transport is not a limitation at a scan rate of 1 mV/s, but transport limitations arise at scan rates of 30 mV/s.

Cyclic voltammetry was also conducted on 347 and 1520 nm thick (PANI $NF_{2.5}/ERGO_{3.5}$) LbL electrodes at varying scan rates (Figure 4c and e, respectively). As scan rate increased from 10 to 100 mV/s, little distortion was observed for the 347 nm thick LbL electrode, and the cathodic peak only slightly shifted from 3 to 2.7 V. The maximum anodic and cathodic currents increased linearly with increasing scan rate, which is suggestive of a nondiffusion-controlled redox process, Figure 4d. In contrast, cyclic voltammograms of 1520 nm thick LbL electrode became distorted, in which the cathodic peak greatly shifted from 2.6 to 1.76 V; further, the maximum current increased nonlinearly with scan rate, Figure 3f. These results are consistent with hindered mass transport in thicker electrodes at high scan rates (100 mV/s). It should be noted that even if the electrode is thick, diffusion limitations can be overcome by charging and discharging at low C-rates.

Journal of Materials Chemistry A

Dynamic Article Links ►

Cite this: DOI: 10.1039/c0xx00000x

ARTICLE

www.rsc.org/xxxxxx

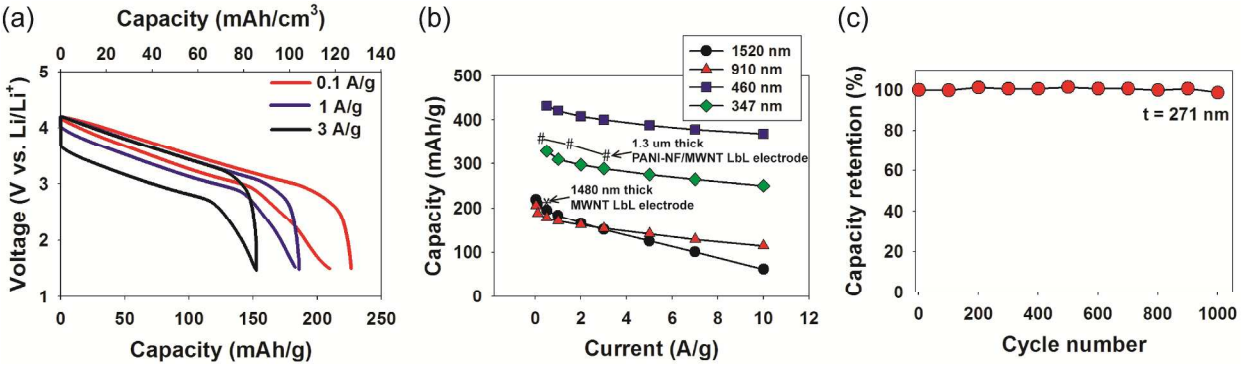

Figure 6. (a) Charge-discharge curves for a 1520 nm thick (PANI $NF_{2.5}/ERGO_{3.5}$) LbL electrode. (b) Capacity of (PANI $NF_{2.5}/ERGO_{3.5}$) LbL electrodes of varying thicknesses *vs.* discharge current. (c) Accelerated cycling behavior of a 271 nm thick (PANI $NF_{2.5}/ERGO_{3.5}$) LbL electrode at 35 A/g. Data in panel (b) are taken from ref.[29, 30] Capacity is based on the LbL mass and volume only.

To further investigate the separate contributions of diffusion-controlled and nondiffusion-controlled charge storage, an additional analysis was performed using following equation:

$$i = av^b \quad (2)$$

where v is the scan rate, i is the current, and a and b are adjustable parameters.[60, 84] If b is 1, the redox process is an ideal nondiffusion-controlled reaction. If b is 0.5, the redox process is an ideal diffusion-controlled process. Intermediate values are indicative of mixed control. The b value was obtained from the slope of a plot of log i *vs.* log v using data from cyclic voltammograms in the range of 1 to 5 mV/s, Figure S9. The b values of 347 and 1520 nm thick (PANI $NF_{2.5}/ERGO_{3.5}$) LbL electrodes are shown for both anodic and cathodic scans (Figure 5a and b, respectively). Both thicknesses showed similar trends in b value. In anodic scans (Figure 5a), the b value increased towards unity and then decreased as voltage increased from 1.5 to 3 V. Around 3 V, b reached minimum values of 0.78 and 0.58 for 347 and 1520 nm thick electrodes, respectively. Above 3 V, b values increased towards unity, which is similar to our previous results for PANI-containing electrodes.[60] In cathodic scans (Figure 5b), the trend in b value was more distinctive depending upon electrode thickness. The b value of the 347 nm thick electrode was near unity above 2.6 V. For the 1520 nm thick electrodes, the b value was between 0.75 and 1 in the range of 2.6 to 4.2 V, which is suggestive of mixed control upon reduction. These results, overall, are consistent with increased diffusion control in the charge storage process for thicker electrodes.

The relative contributions of nondiffusion-controlled and diffusion-controlled charge storage can be further visualized using the following analysis of data obtained from scan rates of 1 to 5 mV/s:

$$i\,(V) = a_1v + a_2v^{0.5} \quad (3)$$

The parameters a_1 and a_2 represent the relative contributions of nondiffusion-controlled and diffusion-controlled processes, respectively.[60, 84] From the slope and the intercept of plots of $i(V)/v^{0.5}$ *vs.* $v^{0.5}$ taken at a specific potential, the parameters a_1 and a_2 were obtained, Figure S10. From these parameters, a cyclic voltammogram such as that shown in Figure 5c-d and Figure S11 was constructed. The solid line represents the combined current for electrodes, and the dotted line shows the current attributed to the diffusion-controlled process. The difference between the two yields the nondiffusion-controlled contribution. Upon comparison, the 1520 nm thick LbL electrode had a larger percentage of diffusion-controlled integrated current as compared to the 347 nm thick electrode (31.4 *vs.* 22.5 %, respectively). This result is in accordance with the results drawn from b value analysis.

Presumably, nondiffusion control arises from some fraction of material that is not readily accessible. The following analysis allows for the separation of the total maximum charge (q_{total}) that can be stored into charge stored at the inner surface (q_{inner}, difficult to be utilized) and the outer surface (q_{outer}, easy to be utilized) by the following equation:[43, 84, 85]

$$q_{total} = q_{inner} + q_{outer} \quad (4)$$

The values of q_{total} and q_{outer} were calculated from the intercept of $1/q$ *vs.* $v^{0.5}$ and q *vs.* $v^{-0.5}$, respectively, for (PANI $NF_{2.5}/ERGO_{3.5}$) LbL electrodes, Figure S12. The percentage of charge stored at inner and outer surfaces was not distinctively dependent on electrode thickness (77 to 86 % from outer surfaces, 14 to 23 % from inner surfaces), Figure 5e. Instead, q_{total} was strongly influenced by film thickness. For example, the 460 nm thick electrode had a q_{total} of 1761 C/g, which consisted of 1390.5 C/g from outer surfaces (easily accessible) and 370.5 C/g from inner surfaces (not easily accessible). In the case of the 1520 nm thick electrode, the capacity of 721.4 C/g was achieved (557.4 C/g from outer surfaces, and 164 C/g from inner surfaces).

Galvanostatic charge-discharge measurements were performed with varying discharge currents on (PANI $NF_{2.5}/ERGO_{3.5}$) LbL electrodes to quantify their capacities and rate capabilities in a three-electrode cell. The charge-discharge profile was typically sloping, a characteristic often observed with conjugated polymers, Figure 6a. The capacity generally decreased with increasing discharge current for all thicknesses investigated, Figure 6b and Table S1. Of the electrodes investigated, the 460 nm thick (PANI $NF_{2.5}/ERGO_{3.5}$) LbL electrode possessed the highest capacity at 0.1 A/g (461 mAh/g and 184 mAh/cm^3) and

Cite this: DOI: 10.1039/c0xx00000x

www.rsc.org/xxxxxx

ARTICLE

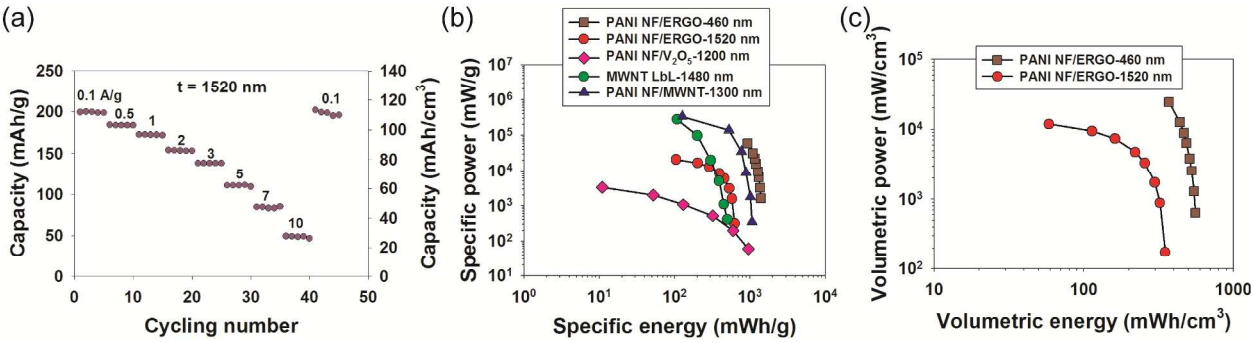

Figure 7. (a) Galvanostatic cycling of a 1520 nm thick (PANI $NF_{2.5}/ERGO_{3.5}$) LbL electrode in a two-electrode sandwich-type cell and Ragone plot based upon the LbL (b) mass and (c) volume. Data in panel (b) were taken from references.[29, 30, 60]

maintained good capacity retention up to 10 A/g (368 mAh/g and 147 mAh/cm^3 or 80 % retention). For comparison, at 0.1 A/g an ERGO electrode had a capacity of 186 mAh/g and PANI NFs alone had a capacity of 195 mAh/g at 0.5 A/g, Table S1. The enhanced porosity of the PANI NF/ERGO electrode perhaps allows for more charge to be stored by the electrical double layer mechanism, thus yielding capacities higher than either material alone. Therefore, the value of 461 mAh/g for a PANI NF/ERGO LbL electrode is consistent with a dual-mode charge storage mechanism and is suggestive of synergistic interactions between the two materials. A similar phenomena has been reported for PANI NF/MWNT LbL electrodes.[30]

In our case, the capacity of (PANI $NF_{2.5}/ERGO_{3.5}$) LbL electrode decreased with increasing thickness, presumably because thinner electrodes are less susceptible to diffusion limitations, Figure 6b and Table S1. The 1520 nm thick LbL electrodes possessed capacity of 210 mAh/g at 0.1 A/g. The capacity decreased from 118 to 35 mAh/cm^3 (210 to 62 mAh/g) when discharge current increased from 0.1 to 10 A/g (30% retention). This specific capacity is similar to that of MWNT LbL electrodes of comparable thickness in a prior report.[29] The (PANI $NF_{2.5}/ERGO_{3.5}$) LbL electrode also exhibited excellent cycling behavior, Figure 6c. After 1000 cycles, 98.7% of the initial capacity was retained. On the contrary, PANI NFs retained only 3 % of its original capacity was retained after 1000 cycles, (Figure S13). This result further supports the idea that complementary interactions are necessary to retain cycling stability in PANI NFs.

Galvanostatic charge-discharge measurements were also performed in two-electrode sandwich-type cells, Figure 7a. The capacity obtained from 1520 nm thick (PANI $NF_{2.5}/ERGO_{3.5}$) LbL electrodes was similar to that observed in the three-electrode configuration. For the sandwich-type cell, the capacity decreased from 112 to 27 mAh/cm^3 (199 to 49 mAh/g) as discharge current increased from 0.1 to 10 A/g. After accelerated cycling at 10 A/g, the original capacity of 199 mAh/g was recovered when 0.1 A/g applied, which highlights the robustness and stability of the (PANI $NF_{2.5}/ERGO_{3.5}$) LbL electrodes. Specific energy and power for 460 and 1520 nm thick (PANI $NF_{2.5}/ERGO_{3.5}$) LbL electrodes are displayed in a Ragone plot along with other previously reported LbL electrodes, Figure 7b.[29, 30, 60] The 460 nm thick electrode possessed higher specific energy and power than the other LbL electrodes. Its maximum specific energy was 1395 mWh/g at a specific power of 1590 mW/g, and a maximum specific power of 60252 mW/g at a specific energy of 927 mWh/g. In the case of the 1520 nm thick (PANI $NF_{2.5}/ERGO_{3.5}$) LbL electrode, at a given specific power of 313 mW/g, its specific energy was comparable to those of MWNT and PANI NF/V_2O_5 LbL electrodes. The specific power of 1520 nm thick (PANI $NF_{2.5}/ERGO_{3.5}$) LbL electrode was higher than that of PANI NF/V_2O_5 LbL electrodes, but lower than that of MWNT LbL electrodes at a given specific energy of 105 mWh/g. Volumetric energy and power of PANI NF/ERGO electrodes are presented in Figure 7c. The 460 nm thick electrode had maximum energy density of 558 mWh/cm^3 at a power density of 636 mW/cm^3. The 1520 nm thick electrode showed maximum energy density of 351 mWh/cm^3 at a given power density of 176 mW/cm^3.

These results show that (PANI $NF_{2.5}/ERGO_{3.5}$) LbL electrodes are favorable as cathodes for thin film batteries. To improve the performance further, it will be necessary to enhance porosity so as to facilitate mass transport and allow for thicker films. As it will be shown in future work, spray-assisted LbL assembly promises to address this need.

Conclusions

The assembly of porous PANI NF/ERGO LbL electrodes was demonstrated. Assembly of GO sheets and subsequent electrochemical reduction circumvented the limited processability of CRGO sheets, which exhibited aggregation during LbL assembly. Electrochemical reduction of GO sheets further eliminates the necessity for harsh reducing agents otherwise required for the synthesis of CRGO. LbL assembly of GO sheets at acidic and at basic pH values with complementary PANI NFs was explored, in which acidic conditions were proven to yield the most robust growth (9.6 nm/layer pair). The resulting electrodes exhibited a low density (0.56 g/cm^3), high void fraction (0.625), and consisted of 81 wt% PANI NFs and 19 wt% GO sheets. Subsequent electrochemical reduction yielded ERGO sheets with

increased sp^2 graphitic domains, confirmed via Raman and X-ray photoelectron spectroscopy. Electrochemical characterization confirmed the enhanced electrochemical activity brought about by electrochemical reduction. Overall the electrodes were reversible over a potential range of 1.5 to 4.2 V *vs.* Li/Li^+. The 460 nm thick (PANI $NF_{2.5}/ERGO_{3.5}$) LbL electrode had one of the highest energy and power values of 546 mWh/cm^3 (1365 mWh/g) at 1284 mW/cm^3 (3209 mW/g) measured at 1 A/g) among previously reported LbL electrodes; further the capacity was exceptionally high (461 mAh/g (184 mAh/cm^3) at 0.1 A/g), originating from redox activity arising from PANI NFs and oxygen-containing functional groups on ERGO sheets, as well as electrical double layer capacitance. Thicker electrodes showed reduced electrochemical activity, presumably because of ion transport limitations. The 1520 nm thick (PANI $NF_{2.5}/ERGO_{3.5}$) LbL electrodes exhibited a capacity of 220 mAh/g (123 mAh/cm^3) at 0.03 A/g. Upon accelerated cycling, (PANI $NF_{2.5}/ERGO_{3.5}$) LbL electrodes retained 98.7% of their initial capacity.

The ease of processing, high capacity, high specific energy and power, and the excellent capacity retention suggest that the (PANI $NF_{2.5}/ERGO_{3.5}$) LbL electrode is an excellent electrode candidate for thin film energy storage, especially as compared to other LbL systems. Our future work will translate this system from dip-assisted LbL assembly to spray-assisted LbL assembly, which is suitable for the rapid build-up of these electrodes over large areas onto a variety of substrates.

Acknowledgements

This work was supported in part by the Air Force Office of Scientific Research (Grant No. FA9550-13-1-0147) and the Welch Foundation (Grant No. A-1766). We thank Dr. M. Akbulut for Zeta-potential access. We also thank TAMU Materials Characterization Facility.

Notes and references

Artie McFerrin Department of Chemical Engineering
Texas A&M University
College Station, Texas 77843. USA
E-mail: Jodie.lutkenhaus@che.tamu.edu

Electronic Supplementary Information (ESI) available: [SEM images of PANI NFs and GO sheets, Zeta potential of GO dispersion, Digital images of (PANI $NF_{2.5}/GO_{3.5}$) LbL films, Adsorbed mass of (PANI $NF_{2.5}/GO_{3.5}$) LbL films using QCM, XPS spectra of PANI NFs and GO sheets, preconditioning of (PANI $NF_{2.5}/ERGO_{3.5}$) LbL electrode, Cyclic voltammograms of (PANI $NF_{2.5}/ERGO_{3.5}$), Cyclic voltammograms of (PANI $NF_{2.5}/ERGO_{3.5}$) LbL electrodes at 30 mV/s, Graph of log i vs. log ν, graph of $i/\nu^{0.5}$ vs. $\nu^{0.5}$, Graphs of 1/q vs. $\nu^{0.5}$ and q vs. $\nu^{-0.5}$, and Capacities of (PANI $NF_{2.5}/ERGO_{3.5}$) at different currents]. See DOI: 10.1039/b000000x/

1. M. Nathan, *Curr. Pharm. Biotechnol.*, 2010, **11**, 404-410.
2. M. Koo, K.-I. Park, S. H. Lee, M. Suh, D. Y. Jeon, J. W. Choi, K. Kang and K. J. Lee, *Nano Letters*, 2012, **12**, 4810-4816.
3. M. Beidaghi and Y. Gogotsi, *Energy & Environmental Science*, 2014, **7**, 867-884.
4. N. J. Dudney and B. J. Neudecker, *Current Opinion in Solid State and Materials Science*, 1999, **4**, 479-482.
5. J. B. Bates, N. J. Dudney, B. Neudecker, A. Ueda and C. D. Evans, *Solid State Ionics*, 2000, **135**, 33-45.
6. Y.-N. Zhou, M.-Z. Xue and Z.-W. Fu, *Journal of Power Sources*, 2013, **234**, 310-332.
7. H. H. Chen, S. Cartmell, Q. Wang, T. Lozano, Z. D. Deng, H. D. Li, X. L. Chen, Y. Yuan, M. E. Gross, T. J. Carlson and J. Xiao, *Sci Rep*, 2014, **4**.
8. F. Albano, Y. S. Lin, D. Blaauw, D. M. Sylvester, K. D. Wise and A. M. Sastry, *Journal of Power Sources*, 2008, **185**, 1524-1532.
9. L. B. Hu, M. Pasta, F. La Mantia, L. F. Cui, S. Jeong, H. D. Deshazer, J. W. Choi, S. M. Han and Y. Cui, *Nano Letters*, 2010, **10**, 708-714.
10. L. B. Hu, J. W. Choi, Y. Yang, S. Jeong, F. La Mantia, L. F. Cui and Y. Cui, *Proc. Natl. Acad. Sci. U. S. A.*, 2009, **106**, 21490-21494.
11. G. M. Zhou, D. W. Wang, F. Li, L. L. Zhang, N. Li, Z. S. Wu, L. Wen, G. Q. Lu and H. M. Cheng, *Chem. Mat.*, 2010, **22**, 5306-5313.
12. R. X. Yu, C. F. Zhang, Q. Meng, Z. X. Chen, H. K. Liu and Z. P. Guo, *ACS Appl. Mater. Interfaces*, 2013, **5**, 12394-12399.
13. A. L. M. Reddy, M. M. Shaijumon, S. R. Gowda and P. M. Ajayan, *Nano Letters*, 2009, **9**, 1002-1006.
14. X. F. Zhou, F. Wang, Y. M. Zhu and Z. P. Liu, *J. Mater. Chem.*, 2011, **21**, 3353-3358.
15. H. L. Wang, Y. Yang, Y. Y. Liang, L. F. Cui, H. S. Casalongue, Y. G. Li, G. S. Hong, Y. Cui and H. J. Dai, *Angew. Chem.-Int. Edit.*, 2011, **50**, 7364-7368.
16. S. H. Ha, Y. S. Jeong and Y. J. Lee, *ACS Appl. Mater. Interfaces*, 2013, **5**, 12295-12303.
17. K. I. Bolotin, K. J. Sikes, Z. Jiang, M. Klima, G. Fudenberg, J. Hone, P. Kim and H. L. Stormer, *Solid State Commun.*, 2008, **146**, 351-355.
18. C. Lee, X. D. Wei, J. W. Kysar and J. Hone, *Science*, 2008, **321**, 385-388.
19. A. A. Balandin, S. Ghosh, W. Z. Bao, I. Calizo, D. Teweldebrhan, F. Miao and C. N. Lau, *Nano Letters*, 2008, **8**, 902-907.
20. M. D. Stoller, S. J. Park, Y. W. Zhu, J. H. An and R. S. Ruoff, *Nano Letters*, 2008, **8**, 3498-3502.
21. F. Schedin, A. K. Geim, S. V. Morozov, E. W. Hill, P. Blake, M. I. Katsnelson and K. S. Novoselov, *Nat. Mater.*, 2007, **6**, 652-655.
22. S. Y. Jang, Y. G. Kim, D. Y. Kim, H. G. Kim and S. M. Jo, *ACS Appl. Mater. Interfaces*, 2012, **4**, 3500-3507.
23. S. Goenka, V. Sant and S. Sant, *J. Control. Release*, 2014, **173**, 75-88.
24. E. Yoo, J. Kim, E. Hosono, H. Zhou, T. Kudo and I. Honma, *Nano Letters*, 2008, **8**, 2277-2282.
25. D. H. Wang, D. W. Choi, J. Li, Z. G. Yang, Z. M. Nie, R. Kou, D. H. Hu, C. M. Wang, L. V. Saraf, J. G. Zhang, I. A. Aksay and J. Liu, *ACS Nano*, 2009, **3**, 907-914.
26. H. X. Ji, L. L. Zhang, M. T. Pettes, H. F. Li, S. S. Chen, L. Shi, R. Piner and R. S. Ruoff, *Nano Letters*, 2012, **12**, 2446-2451.
27. B. G. Choi, M. Yang, W. H. Hong, J. W. Choi and Y. S. Huh, *ACS Nano*, 2012, **6**, 4020-4028.
28. S. Stankovich, D. A. Dikin, R. D. Piner, K. A. Kohlhaas, A. Kleinhammes, Y. Jia, Y. Wu, S. T. Nguyen and R. S. Ruoff, *Carbon*, 2007, **45**, 1558-1565.
29. S. W. Lee, N. Yabuuchi, B. M. Gallant, S. Chen, B. S. Kim, P. T. Hammond and Y. Shao-Horn, *Nat. Nanotechnol.*, 2010, **5**, 531-537.
30. M. N. Hyder, S. W. Lee, F. C. Cebeci, D. J. Schmidt, Y. Shao-Horn and P. T. Hammond, *ACS Nano*, 2011, **5**, 8552-8561.
31. H. R. Byon, S. W. Lee, S. Chen, P. T. Hammond and Y. Shao-Horn, *Carbon*, 2011, **49**, 457-467.
32. S. W. Lee, B. M. Gallant, H. R. Byon, P. T. Hammond and Y. Shao-Horn, *Energy Environ. Sci.*, 2011, **4**, 1972-1985.
33. H. Kim, K.-Y. Park, J. Hong and K. Kang, *Sci. Rep.*, 2014, **4**.
34. K. S. Novoselov, A. K. Geim, S. V. Morozov, D. Jiang, Y. Zhang, S. V. Dubonos, I. V. Grigorieva and A. A. Firsov, *Science*, 2004, **306**, 666-669.
35. K. S. Kim, Y. Zhao, H. Jang, S. Y. Lee, J. M. Kim, J. H. Ahn, P. Kim, J. Y. Choi and B. H. Hong, *Nature*, 2009, **457**, 706-710.
36. S. Park, J. H. An, I. W. Jung, R. D. Piner, S. J. An, X. S. Li, A. Velamakanni and R. S. Ruoff, *Nano Letters*, 2009, **9**, 1593-1597.
37. X. Y. Yang, X. Dou, A. Rouhanipour, L. J. Zhi, H. J. Rader and K. Mullen, *J. Am. Chem. Soc.*, 2008, **130**, 4216-+.

38. Y. Su, X. Gao and J. Zhao, *Carbon*, 2014, **67**, 146-155.
39. D. Li, M. B. Muller, S. Gilje, R. B. Kaner and G. G. Wallace, *Nat. Nanotechnol.*, 2008, **3**, 101-105.
40. Y. Shao, J. Wang, M. Engelhard, C. Wang and Y. Lin, *J. Mater. Chem.*, 2010, **20**, 743-748.
41. H. L. Guo, X. F. Wang, Q. Y. Qian, F. B. Wang and X. H. Xia, *ACS Nano*, 2009, **3**, 2653-2659.
42. J. F. Mike and J. L. Lutkenhaus, *Journal of Polymer Science Part B-Polymer Physics*, 2013, **51**, 468-480.
43. L. Shao, J. W. Jeon and J. L. Lutkenhaus, *Chem. Mat.*, 2012, **24**, 181-189.
44. J. X. Huang and R. B. Kaner, *Angew. Chem.-Int. Edit.*, 2004, **43**, 5817-5821.
45. D. Li and R. B. Kaner, *Chem. Commun.*, 2005, 3286-3288.
46. F. Cheng, W. Tang, C. Li, J. Chen, H. Liu, P. Shen and S. Dou, *Chemistry – A European Journal*, 2006, **12**, 3082-3088.
47. S. Taguchi and T. Tanaka, *Journal of Power Sources*, 1987, **20**, 249-252.
48. J. W. Jeon, J. O'Neal, L. Shao and J. L. Lutkenhaus, *ACS Appl. Mater. Interfaces*, 2013, **5**, 10127-10136.
49. M. N. Hyder, B. M. Gallant, N. J. Shah, Y. Shao-Horn and P. T. Hammond, *Nano Letters*, 2013, **13**, 4610-4619.
50. A. K. Sarker and J. D. Hong, *Langmuir*, 2012, **28**, 12637-12646.
51. A. K. Sarker and J. D. Hong, *Colloid Surf. A-Physicochem. Eng. Asp.*, 2013, **436**, 967-974.
52. G. Decher, *Science*, 1997, **277**, 1232-1237.
53. S. S. Shiratori and M. F. Rubner, *Macromolecules*, 2000, **33**, 4213-4219.
54. S. T. Dubas and J. B. Schlenoff, *Macromolecules*, 1999, **32**, 8153-8160.
55. K. Müller, J. F. Quinn, A. P. R. Johnston, M. Becker, A. Greiner and F. Caruso, *Chem. Mat.*, 2006, **18**, 2397-2403.
56. C. Sung, K. Hearn, D. K. Reid, A. Vidyasagar and J. L. Lutkenhaus, *Langmuir*, 2013, **29**, 8907-8913.
57. J. L. Lutkenhaus, K. D. Hrabak, K. McEnnis and P. T. Hammond, *Journal of the American Chemical Society*, 2005, **127**, 17228-17234.
58. C. Y. Cho, L. Valverde, G. A. Ozin and N. S. Zacharia, *Langmuir*, 2010, **26**, 13637-13643.
59. X. Li, D. Hu, K. Huang and C. Yang, *Journal of Materials Chemistry A*, 2014, **2**, 11830-11838.
60. L. Shao, J. W. Jeon and J. L. Lutkenhaus, *Journal of Materials Chemistry A*, 2013, **1**, 7648-7656.
61. Z. Gao, W. L. Yang, J. Wang, H. J. Yan, Y. Yao, J. Ma, B. Wang, M. L. Zhang and L. H. Liu, *Electrochim. Acta*, 2013, **91**, 185-194.
62. S. W. Lee, B. S. Kim, S. Chen, Y. Shao-Horn and P. T. Hammond, *J. Am. Chem. Soc.*, 2009, **131**, 671-679.
63. M. Schnippering, H. V. Powell, S. R. Mackenzie and P. R. Unwin, *J. Phys. Chem. C*, 2009, **113**, 20221-20227.
64. S. Stankovich, D. A. Dikin, G. H. B. Dommett, K. M. Kohlhaas, E. J. Zimney, E. A. Stach, R. D. Piner, S. T. Nguyen and R. S. Ruoff, *Nature*, 2006, **442**, 282-286.
65. J. Stejskal, I. Sapurina, J. Prokes and J. Zemek, *Synth. Met.*, 1999, **105**, 195-202.
66. B. Stevens, E. Dessiatova, D. A. Hagen, A. D. Todd, C. W. Bielawski and J. C. Grunlan, *ACS Appl. Mater. Interfaces*, 2014, **6**, 9942-9945.
67. J. X. Huang and R. B. Kaner, *Journal of the American Chemical Society*, 2004, **126**, 851-855.
68. M. S. Dresselhaus, A. Jorio, M. Hofmann, G. Dresselhaus and R. Saito, *Nano Letters*, 2010, **10**, 751-758.
69. J. W. Jeon, R. Sharma, P. Meduri, B. W. Arey, H. T. Schaef, J. L. Lutkenhaus, J. P. Lemmon, P. K. Thallapally, M. I. Nandasiri, B. P. McGrail and S. K. Nune, *ACS Appl. Mater. Interfaces*, 2014, **6**, 7214-7222.
70. H. L. Wang, Q. L. Hao, X. J. Yang, L. D. Lu and X. Wang, *Nanoscale*, 2010, **2**, 2164-2170.
71. E. Y. Choi, T. H. Han, J. H. Hong, J. E. Kim, S. H. Lee, H. W. Kim and S. O. Kim, *J. Mater. Chem.*, 2010, **20**, 1907-1912.
72. S. M. Bak, K. W. Nam, C. W. Lee, K. H. Kim, H. C. Jung, X. Q. Yang and K. B. Kim, *J. Mater. Chem.*, 2011, **21**, 17309-17315.
73. J. F. Che, L. Y. Shen and Y. H. Xiao, *J. Mater. Chem.*, 2010, **20**, 1722-1727.
74. H. K. Jeong, Y. P. Lee, R. Lahaye, M. H. Park, K. H. An, I. J. Kim, C. W. Yang, C. Y. Park, R. S. Ruoff and Y. H. Lee, *J. Am. Chem. Soc.*, 2008, **130**, 1362-1366.
75. T. Szabó, O. Berkesi, P. Forgó, K. Josepovits, Y. Sanakis, D. Petridis and I. Dékány, *Chem. Mat.*, 2006, **18**, 2740-2749.
76. H.-J. Shin, K. K. Kim, A. Benayad, S.-M. Yoon, H. K. Park, I.-S. Jung, M. H. Jin, H.-K. Jeong, J. M. Kim, J.-Y. Choi and Y. H. Lee, *Adv. Funct. Mater.*, 2009, **19**, 1987-1992.
77. S. Golczak, A. Kanciurzewska, M. Fahlman, K. Langer and J. J. Langer, *Solid State Ionics*, 2008, **179**, 2234-2239.
78. X. Q. Jiang, S. Setodoi, S. Fukumoto, I. Imae, K. Komaguchi, J. Yano, H. Mizota and Y. Harima, *Carbon*, 2014, **67**, 662-672.
79. I. Jung, D. A. Field, N. J. Clark, Y. W. Zhu, D. X. Yang, R. D. Piner, S. Stankovich, D. A. Dikin, H. Geisler, C. A. Ventrice and R. S. Ruoff, *J. Phys. Chem. C*, 2009, **113**, 18480-18486.
80. A. Ganguly, S. Sharma, P. Papakonstantinou and J. Hamilton, *J. Phys. Chem. C*, 2011, **115**, 17009-17019.
81. Y. Gogotsi and P. Simon, *Science*, 2011, **334**, 917-918.
82. S. Y. Kim, J. Hong, R. Kavian, S. W. Lee, M. N. Hyder, Y. Shao-Horn and P. T. Hammond, *Energy Environ. Sci.*, 2013, **6**, 888-897.
83. J.-W. Jeon, Y. Ma, J. F. Mike, L. Shao, P. B. Balbuena and J. L. Lutkenhaus, *Phys. Chem. Chem. Phys.*, 2013, **15**, 9654-9662.
84. M. Sathiya, A. S. Prakash, K. Ramesha, J. M. Tarascon and A. K. Shukla, *J. Am. Chem. Soc.*, 2011, **133**, 16291-16299.
85. S. Ardizzone, G. Fregonara and S. Trasatti, *Electrochim. Acta*, 1990, **35**, 263-267.

Graphical Abstract

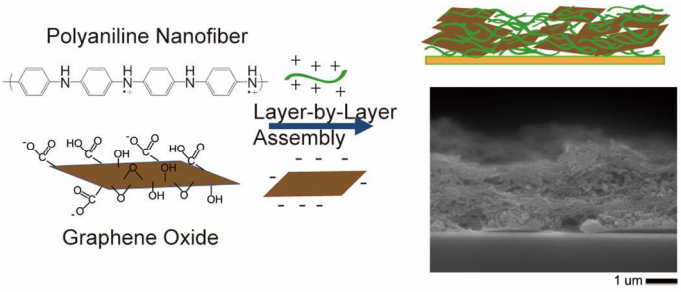

The layer-by-layer assembly of graphene oxide sheets and polyaniline nanofibers, followed by electrochemical reduction, results in highly porous electroactive electrodes for energy storage.